Article

Parallel Allostery by cAMP and PDE Coordinates Activation and Termination Phases in cAMP Signaling

Srinath Krishnamurthy,[1] Nikhil Kumar Tulsian,[1] Arun Chandramohan,[1] and Ganesh S. Anand[1,*]
[1]Department of Biological Sciences, National University of Singapore, Singapore

ABSTRACT The second messenger molecule cAMP regulates the activation phase of the cAMP signaling pathway through high-affinity interactions with the cytosolic cAMP receptor, the protein kinase A regulatory subunit (PKAR). Phosphodiesterases (PDEs) are enzymes responsible for catalyzing hydrolysis of cAMP to 5′ AMP. It was recently shown that PDEs interact with PKAR to initiate the termination phase of the cAMP signaling pathway. While the steps in the activation phase are well understood, steps in the termination pathway are unknown. Specifically, the binding and allosteric networks that regulate the dynamic interplay between PKAR, PDE, and cAMP are unclear. In this study, PKAR and PDE from *Dictyostelium discoideum* (R_D and RegA, respectively) were used as a model system to monitor complex formation in the presence and absence of cAMP. Amide hydrogen/deuterium exchange mass spectrometry was used to monitor slow conformational transitions in R_D, using disordered regions as conformational probes. Our results reveal that R_D regulates its interactions with cAMP and RegA at distinct loci by undergoing slow conformational transitions between two metastable states. In the presence of cAMP, R_D and RegA form a stable ternary complex, while in the absence of cAMP they maintain transient interactions. RegA and cAMP each bind at orthogonal sites on R_D with resultant contrasting effects on its dynamics through parallel allosteric relays at multiple important loci. R_D thus serves as an integrative node in cAMP termination by coordinating multiple allosteric relays and governing the output signal response.

INTRODUCTION

Signaling pathways are exquisitely regulated by a complex interplay of reversible interactions with partner proteins, ligand cofactors, and posttranslational modifications. These multivalent interactions modulate the cell's spatiotemporal recognition of and response to extracellular stimuli. Signaling pathways are also characterized by distinct activation and termination phases that govern the duration, intensity, and amplification of the signal as it is propagated through the cell (1). Signaling proteins are intrinsically dynamic and populate multiple conformational states in equilibrium and its ligands/partner proteins alter these conformational equilibria (2–4). Indeed, an overlay of protein dynamics is fundamental for bridging structure and function of signaling proteins and consequently for a molecular understanding of signal transduction (5–7). Reversible protein ligand and protein-protein interactions play a critical role in altering dynamic properties of signaling molecules. At a molecular level, signals mediated by specific ligands or partner proteins are propagated across the target protein from active sites to effector sites through allostery. This allosteric communication from one protein locus to another constitutes the basis of signaling proteins' function (8,9). Consequently, signaling proteins have distinct loci for binding diverse ligands and partner proteins and these sites are allosterically coupled (10). An emerging challenge in protein chemistry lies in delineating binding interactions from long-range propagation of multivalent allosteric relays in signaling proteins.

Amide hydrogen/deuterium exchange mass spectrometry (HDXMS) has emerged as a powerful tool for mapping allosteric communication in proteins (11,12). The method relies on tracking the acid- and base-catalyzed abstraction of protein backbone amides and replacement by different protons. The rate of amide exchange is dependent on solvent accessibility as well as H-bond propensities and strengths and provides an overview of protein dynamics (13). In addition to mapping allosteric changes in proteins (14,15), HDXMS also has been useful for mapping dynamics of transient interactions in ternary complexes of multiple proteins with ligands and for monitoring progression of enzyme reactions in solution (16). In this study, we set out to apply HDXMS to characterize protein-ligand interactions and map associated allosteric networks in the second messenger cyclic AMP (cAMP)/protein kinase A (PKA) signaling pathway. In this pathway, a single protein (regulatory subunit) functions as a cAMP receptor and interacts with two important effector proteins: the kinase (catalytic subunit) and a phosphodiesterase (PDE) (17–19). In this study we describe how this protein functions as an integrative node in the signaling pathway by responding allosterically in myriad

Submitted March 20, 2015, and accepted for publication June 25, 2015.

*Correspondence: dbsgsa@nus.edu.sg

Srinath Krishnamurthy and Nikhil Kumar Tulsian contributed equally to this work.

Editor: Jason Kahn.

0006-3495/15/09/1251/13

http://dx.doi.org/10.1016/j.bpj.2015.06.067

ways to cAMP and two antagonistic effector proteins to modulate the output response.

The second messenger 3′, 5′- cyclic adenosine monophosphate (cyclic AMP) transduces the effects of external hormonal stimulation and mediates a myriad of intracellular responses. In *Dictyostelium discoideum*, cAMP is both a chemoattractant and intracellular signaling molecule (20,21). Its most profound role is in initiating important physiological changes associated with transformation from a unicellular to a multicellular state in response to starvation (22,23). One of the main targets of cAMP is cyclic AMP-dependent protein kinase, also referred to as PKA, which consists of catalytic (C) and regulatory (R) subunits. In the absence of cAMP, PKA exists as an inactive complex of R- and C-subunits (referred to as the holoenzyme) (24). cAMP binding to the holoenzyme induces conformational changes and facilitates the release of the active C-subunit (17,25,26). This constitutes the activation phase of the cAMP signaling pathway. PDEs, enzymes responsible for catalyzing hydrolysis of cAMP to 5′AMP, initiate the termination phase of the cAMP signaling pathway by forming direct interactions with the cyclic-nucleotide-binding (CNB) pocket domains of PKA R-subunit and hydrolyzing the bound cAMP (Fig. 1 *A*) (19,27). The R-subunit of *D. discoideum* (henceforth referred to as R_D) differs from its mammalian homologs in being monomeric, and lacks an N-terminal dimerization domain, but contains two canonical cyclic AMP binding sites in two distinct domains, CNB domains A and B (denoted CNB:A and CNB:B) (Fig. 1 *B*) (28–30). The CNB domains have a conserved fold with a cAMP binding site containing a characteristic motif for cAMP binding (Fig. 1 *B*, *inset*). The binding site forms a buried pocket shielding cAMP

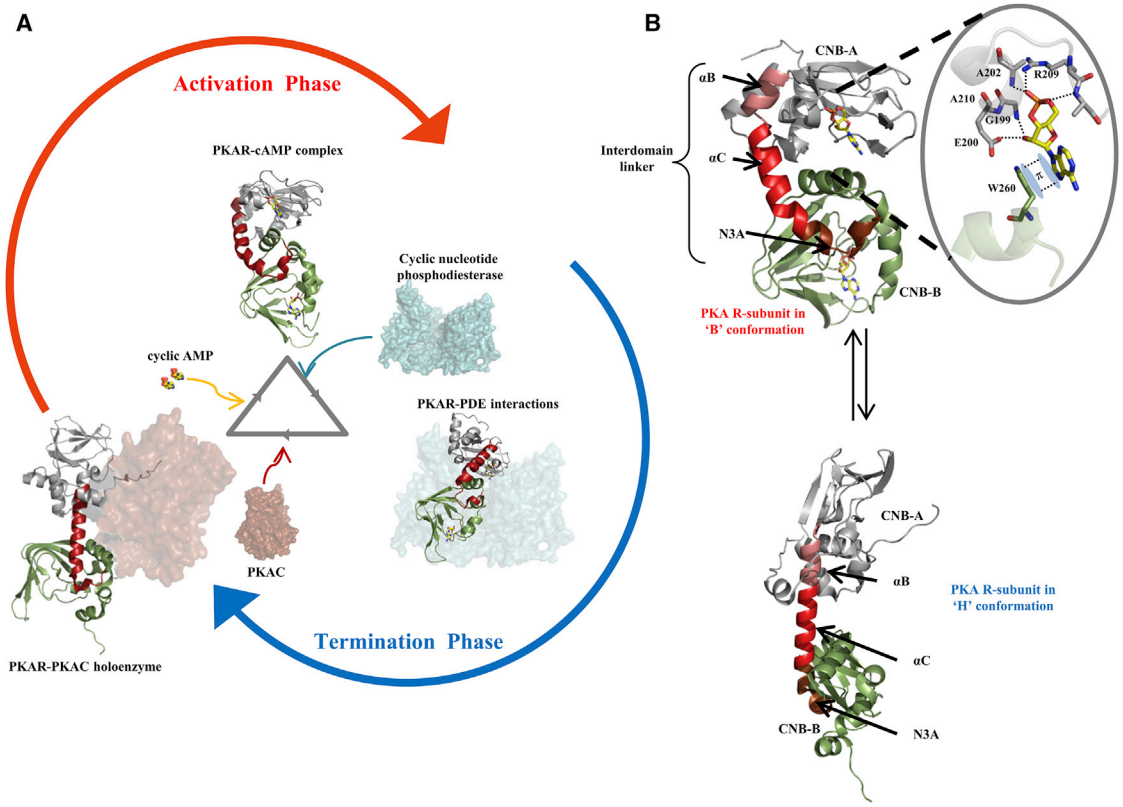

FIGURE 1 Dynamic modulators of PKA regulatory subunit in cAMP signaling pathway. (*A*) The PKAR exhibits multiple end-point conformations in the course of the cAMP signaling pathway. Here PKAR is represented in cartoon form with (*gray*) CNB:A domain and (*green*) CNB:B domain, with the dynamic interdomain linker (B/C helix) (*red*) and cAMP (*yellow sticks*). In its inactive form, PKAR binds to PKA catalytic subunit (PKAC, *brown surface representation*) to form the inactive holoenzyme complex (H form) (PDB: 2QCS). In this form, PKAR is in an extended form. cAMP (*yellow sphere representation*) binds to PKAR, which in turn releases and activates PKAC. In the cAMP-bound form (B form), PKAR adopts a compact conformation (PDB: 1RGS). The transition from holoenzyme form to the cAMP-bound form constitutes the activation phase of the cAMP signaling pathway. In the termination phase, cyclic nucleotide PDEs form direct interactions with cAMP-bound PKAR (docking model (27)) and cause the release and dissociation of bound cAMP. Free PKAR can now bind PKAC and regenerate the holoenzyme, thereby terminating the cAMP pathway. PKAR is a dynamic protein and its conformations are modulated by PKAC, cAMP, and PDEs in different stages of the cAMP signaling pathway. (*B*) The interdomain linker is important in conformational transitions of PKAR from the cAMP-bound B form and the holoenzyme H form. The interdomain linker is composed of the α:B helix (in *salmon*), α:C helix (in *red*), and N3A helix (in *brown*). In the B form, the linker is kinked into three distinct segments, while in the H form, the linker adopts an extended helical conformation. Also depicted are the interactions that cAMP makes with residues in the cAMP binding pocket of CNB:A in PKAR (*inset*). Multiple hydrogen bonds (*dotted lines*) along with π stacking between W260 and the adenine ring of cAMP secure the molecule in the binding pocket.

from the action of phosphodiesterases (31). Previous studies have shown that in R_D, CNB:A binds to cAMP with high affinity, while cAMP binding to CNB:B has not been detected and assumed to be a low-affinity site, despite having all the motifs typical of high-affinity cAMP binding domains across PKA R-subunits (28,30).

R_D is the primary receptor of cAMP and mediates multivalent interactions with the C-subunit and phosphodiesterases. The *D. discoideum* phosphodiesterase RegA, important in different stages of cell development, was shown to interact with PKA R-subunit and control PKA-mediated differentiation of prestalk and spore cells, and regulate encystation (22). We have earlier shown that the catalytic domain of RegA ($RegA_C$) is sufficient for hydrolysis of cAMP tightly bound to the mammalian R-subunit (19). Distinct conformations of mammalian R-subunit have been captured by crystallography (32) and NMR (33–35) and the endpoint states have been denoted as B (cAMP-bound) and H (C-subunit or inactive) forms (36). These conformational transitions have been the focus of several studies to map the allosteric transitions in response to cAMP and C-subunit binding (33,37,38). There have been far fewer studies on how PDEs interact to hydrolyze cAMP bound to PKA R-subunit and initiate cAMP signal termination (19,27). Further, how signals in the cAMP signaling pathway converge and branch off from a target through alternate allosteric pathways is of enormous interest. R_D is the primary cAMP receptor and a great model system for mapping interactions with ligand, cAMP, and partner proteins ($RegA_C$). This has been achieved using HDXMS, which allows monitoring cAMP through the activation and termination phases of the pathway by following backbone amide hydrogens as reporters across R_D. In the course of following cAMP, we also describe binding and allosteric networks associated with signal termination in cAMP signaling mediated via R_D-$RegA_C$-cAMP interactions.

Our results reveal how cAMP and the effector protein, $RegA_C$, interact with R_D at spatially distal sites, allosterically coupled to regulate the output response. We describe how PDEs access cAMP bound to the receptor, R-subunit, to mediate signal termination in cAMP signaling. We show that effects of cAMP binding and PDE interactions are transmitted through distinct, nonoverlapping allosteric relays. This underscores how the intracellular cAMP receptor, R_D, functions as an integrative node by mediating multiple interactions with effector proteins, to regulate the output response.

MATERIALS AND METHODS

Materials

A plasmid encoding full-length R_D with codon optimization for *Escherichia coli* expression was obtained from DNA2.0 (Menlo Park, CA). Chemically competent *E. coli* BL21 (DE3) bacterial strains were from Life Technologies (Carlsbad, CA). TALON Cobalt affinity resin for His-tag purification was from Clontech (Mountain View, CA). LC/MS grade acetonitrile and water were from Fisher Scientific (Waltham, MA). Poroszyme immobilized pepsin cartridge was from Applied Biosystems (Foster City, CA); deuterium oxide (99.9%) was from Cambridge Isotope Laboratories (Tewksbury, MA). All other reagents were research grade from Sigma-Aldrich (St. Louis, MO).

Protein expression and purification

R_D was first subcloned into pET28a plasmid and transformed into *E. coli* BL21 (DE3) for bacterial expression and purification. Bacterial cell pellet (15 g) was subject to sonication in lysis buffer (20 mM Tris-HCl pH 7.5, 100 mM NaCl, and 5 mM β-mercaptoethanol) for 20 min. Lysate was centrifuged at 17,000 $\times$ *g* for 30 min and supernatant was then incubated with Cobalt metal affinity chromatography resin for 1 h. R_D was eluted in lysis buffer containing 300 mM imidazole. Eluate was subsequently subjected to size-exclusion chromatography on a Superdex S-200 column (GE Healthcare Life Sciences, Marlborough, MA) as a finishing step. Purity of the purified R_D was confirmed by sodium dodecyl sulfate-polyacrylamide gel electrophoresis. We factor that cAMP in *E. coli* would bind R_D during expression and this dissociates during size-exclusion chromatography to generate apo R_D. GST-tagged catalytic domain of RegA ($RegA_C$) was purified as previously described in Moorthy et al. (19). Briefly, GST-tagged $RegA_C$ was overexpressed in *E. coli* BL21 (DE3) and purified using glutathione sepharose 4B resin-based (GE Healthcare Life Sciences) affinity chromatography followed by size-exclusion chromatography.

Isothermal titration calorimetry

Isothermal titration calorimetry (ITC) measurements were carried out to monitor the binding and determine the dissociation constant of cAMP and RegAc to apo R_D protein using a VP-ITC MicroCalorimeter (MicroCal, Northampton, MA). The cell reservoir was filled with 1.8 mL of 10 μM R_D protein, reference cell with 1.8 mL of buffer (20 mM Tris-Cl pH 7.5, 100 mM NaCl) and syringe with final volume ~400 μL of 200 μM cAMP prepared in the same buffer. The binding reaction was started with first injection volume of 2 μL followed by 39 sequential injections each of 4 μL cAMP at intervals of 240 s and set to stirring speed of 350 rpm. Continuous measurement of heat change inside the cell allowed determination of enthalpy change during the process ΔH (-53.7 kcal/mol $\pm$ 1.6 kcal/mol) and the equilibrium association constant K_A ($9.92 \times 10^5 \pm 1.02 \times 10^4$ M^{-1}, dissociation constant (K_D) ~1 μM. Three independent titration experiments were carried out at 298 K with similar results and a representative ITC graph is depicted in Fig. S2 in the Supporting Material. Similar experiments were carried out for probing binding of $RegA_C$ to R_D (data not shown).

Amide hydrogen/deuterium exchange mass spectrometry

Deuterium exchange experiments were first carried out on cAMP-free (*apo*) R_D (4 μM final concentration). To test effects of cAMP on R_D dynamics, cAMP at final reaction concentration of 300 μM, was added to apo R_D. This high concentration of cAMP was used to fully saturate the CNB:A site and possibly the CNB:B site, which has been predicted to not bind at lower ($<\mu$M) concentrations of cAMP (28). To capture dynamics of apo R_D in a binary complex with $RegA_C$, $RegA_C$ (2 μM) was complexed with apo R_D (6 μM) in a 1:3 molar ratio of $RegA_C$ to R_D. A ternary complex of R_D, cAMP, and $RegA_C$ was obtained by complexing $RegA_C$ (2 μM) with apo R_D (6 μM) in the presence of 300 μM cAMP. In all conditions, complexation reaction was initiated simultaneously with the deuterium exchange reaction in the presence of deuterated buffer.

Buffer for deuterium exchange reaction was prepared by vacuum evaporation of aqueous buffer (20 mM Tris-HCl pH 7.5, 100 mM NaCl) until dry,

which was subsequently reconstituted in 99.9% D_2O. The deuterium exchange reaction was initiated by diluting the sample 10-fold in deuterated exchange buffer (20 mM Tris-HCl pH 7.5, 100 mM NaCl) resulting in a final deuterium concentration of 90% in the deuterium labeling reaction. The deuterium-oxide-exchanged buffer was maintained at a final pH_{read} of 7.5. Deuterium exchange reactions were carried out for the following times: 30 s, and 1, 5, 10, 30, 60, and 100 min. The exchange reaction was quenched by lowering the pH_{read} of the reaction to 2.5, using 0.1% trifluoro acetic acid. Samples were injected onto a nano-UPLC HDX sample manager (Waters, Milford, MA) as described in Wales et al. (39). Online immobilized pepsin digestion and reverse phase liquid chromatography were carried out as previously described in Krishnamurthy et al. (27). Peptides separated from previous liquid chromatography were subsequently sprayed onto a SYNAPT G2-Si mass spectrometer (Waters) acquiring in MS^E mode. Continuous instrument calibration was carried out using Glu-fibrinogen peptide, according to manufacturer's recommendations. Back-exchange factor for the system was found on average to be ~30% (19), but in this study only the uncorrected raw values are reported.

Peptide identification and mass spectral data analysis

Peptides from MS^E spectra of undeuterated samples were identified using PROTEIN LYNX GLOBAL SERVER, Ver. 3.0 (Waters). Deuterium exchange data was quantified by DYNAMX software (Ver. 2.0, Waters). The reported values are an average of three independent hydrogen/deuterium exchange experiments (Table S1 in the Supporting Material). Peptides showing EX1 kinetics of amide exchange were additionally analyzed using GRAPHPAD PRISM 6.0 (San Diego, CA). The bimodal deconvolutions were carried out by fitting the curves to a sum of Gaussian equation. Amplitudes and centroid values for each deconvoluted envelope are reported in Table S2.

RESULTS

R_D CNB:B domain exhibits distinct HDX bimodal spectra consistent with local unfolding

It has been previously shown that the mammalian PKA R-subunit is an intrinsically dynamic protein that forms high-affinity complexes with cAMP (K_D ~ nM), and cAMP-mediated allostery in the R-subunit has been explained by conformational selection (36). PKA is a highly conserved protein widely found in all eukaryotes (40,41), and we hypothesized that R_D from *D. discoideum* with ~51% sequence homology with mammalian PKA regulatory domain isoform Iα would exhibit similar dynamic properties to its mammalian homolog. To test this, we first set out to characterize protein dynamics of apo R_D. HDXMS experiments of apo R_D were carried out as described in the Materials and Methods and a total of 24 peptides was identified and analyzed, corresponding to ~71% of the primary sequence of R_D (Fig. S1). The overall dynamic profile of R_D is provided in a relative exchange plot (Fig. 2 *A*). A relative exchange plot is a plot of the ratio of average deuterons exchanged to the total number of exchangeable amides available for each peptide. Regions of the protein that are dynamic in nature have higher relative deuterium uptake values.

Closer examination of the mass spectral envelopes of all peptides revealed that three regions showed a bimodal distribution of mass spectra (Fig. 2 *B*). Bimodal distributions are characterized by the presence of multiple spectral envelopes within the same mass spectrum. The most common reason for the presence of bimodal spectra in HDXMS experiments is attributed to the EX1 deuterium exchange regime (42,43). EX1 kinetics are rarely seen in soluble proteins at physiological conditions and are indicative of local unfolding events coupled to slow conformational changes (11,13,44). They also report on the dynamic interconversion between alternate population states of the protein (45). EX1 kinetics can serve as conformational probes and provide important insights into protein dynamics and function (44,46). Mass spectra from shorter deuterium exchange labeling time experiments (30 s to 5 min) exhibited bimodal characteristics, but as labeling time increased, the bimodality of the spectrum decreased and shifted toward a binomial spectrum. These phenomena are typical of EX1 kinetics in HDXMS experiments (47). The peptides exhibiting bimodal distribution were found to span loci important for R_D function, mainly the putative C-helix (Residues 171–201) and the conserved arginine containing the CNB region in domain B (Residues 266–279) (48). Deconvolution of the bimodal spectral envelopes confirmed EX1 kinetics, and the interpretation of these results is described in a later section (see Fig. 6 *A*). A peptide spanning residues 191–201 is binomial in nature (data not shown), thus by subtractive analysis we can localize the region showing bimodal distribution to the residues 171–190. To better visualize these results, the results were mapped onto the three-dimensional model of R_D (Fig. 2 *C*). A structural model for R_D was generated using the structure of a close homolog, PKA RIα from *Bos taurus* (PDB: 1RGS) using SWISS-MODELER (http://swissmodel.expasy.org/).

HDX bimodal signatures as conformational probes to monitor perturbations in protein dynamics

Our results indicated at least three distinct loci showing bimodal kinetics of deuterium exchange and therefore highlighting these sites as undergoing slow conformational transitions in apo R_D. We next examined the effects of cAMP on the overall dynamics of R_D, including the above loci by HDXMS analysis of R_D, in the presence of 300 μM cAMP. Like other regulatory subunits from homologous protein kinases, the R_D CNB:A site has been shown to have a high affinity for cAMP with a dissociation constant in nanomolar range, K_D = ~3 nM (29,49). On the other hand, the binding affinity of cAMP at the CNB:B site, measured using isothermal titration calorimetry, was found to be K_D ~1 μM (Fig. S2). Knowledge of the binding constants guided concentrations of cAMP used (300 μM) in the HDXMS experiments to ensure ligand saturation of the cAMP binding pocket at both the high-affinity CNB:A and the low-affinity CNB:B domains in the HDXMS experiments.

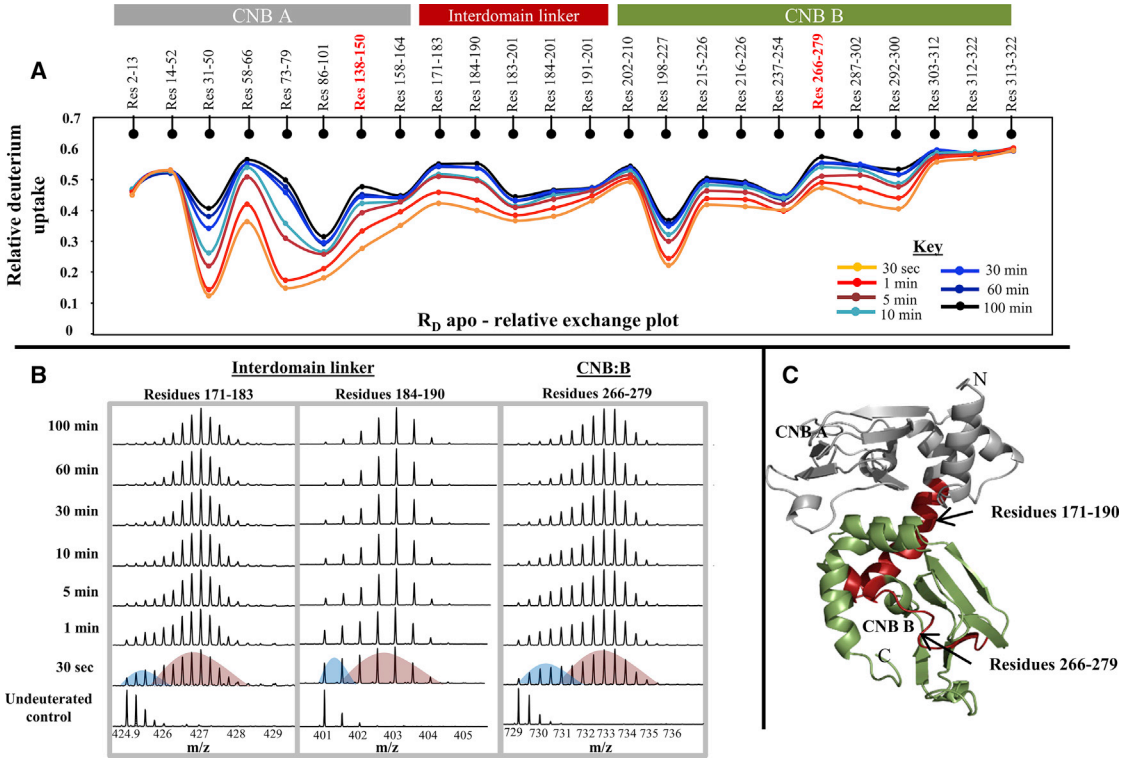

FIGURE 2 Apo R_D is a dynamic protein with regions that undergo slow structural transitions/local unfolding. (*A*) The relative deuterium uptake value (calculated as the ratio of average deuterium ions exchanging to the maximum exchangeable amides; *y* axis) for each pepsin digest fragment from the N- to C-terminus (*x* axis) of R_D is plotted in a relative exchange plot. The relative exchange plot provides a snapshot of the overall dynamics of R_D for each deuterium labeling time point as depicted in the key. Peptides spanning the cAMP binding pocket in CNB A and B are highlighted (*red*). Plots were generated using the software DYNAMX. (*B*) Stacked mass spectra of the three peptides exhibiting bimodal distributions are shown. Mass spectra are stacked in order of increasing deuterium labeling time (*y* axis) as shown. Colored curves are used to represent lower-exchanging (*blue curve*) and higher-exchanging (*red curve*) distributions in the 30-s labeling time of spectra. (*C*) Peptides showing bimodal characteristics are mapped (*red*) onto the modeled structure of R_D. (*Gray*) CNB:A (residues 1–180) and (*green*) CNB:B (residues 181–327); the N- and C-termini of the protein and CNB pocket in A and B domains are labeled.

Results from cAMP-bound R_D were compared with apo R_D and revealed three regions showing significant differences in deuterium exchange. A difference plot depicting differences between apo R_D and R_D:cAMP is shown in Fig. 3 *A*. This plot shows the average difference between the two states for each peptide and deuterium labeling time. The average error between replicate runs for each peptide was between 0.1 and 0.2 Da in our experimental setup, and a difference of 0.5 Da or more is considered significant (50). Two of the three regions showed significant decreases in deuterium exchange and are located within the cAMP binding pockets of CNB:A and CNB:B, respectively. A third region spanning residues 287–302 also showed significant differences at shorter deuterium labeling times, but at increased labeling times the difference between apo R_D and R_D:cAMP were negligible. This region is distal to both cAMP binding pockets and represents an allosteric effect upon ligand binding. We also observed increased deuterium exchange in a peptide spanning residues 31–50, which flanks the putative PKAC binding site. These results are mapped onto the modeled structure of R_D in Fig. 3 *B*. Representative mass spectra for peptides in CNB:A and CNB:B are shown in Fig. 3 *C*.

Of the three peptides showing bimodal kinetics of deuterium exchange in apo R_D, only one of the peptides spanning residues 266–279 at CNB:B showed differences in the presence of cAMP. The spectrum exhibited sharper bimodal characteristics, resulting in a shift of the centroid to the left (Fig. 3 *C ii*). This bimodal distribution is seen for the entire time course of the deuterium-labeling experiment. Interestingly, the centroid of the higher-exchanging population did not show any shifts, but the centroid of the lower-exchanging population shifted to the right with increasing labeling time (see Fig. 6 *B*). The spectra for the lower-exchanging species are representative of EX2 deuterium exchange kinetics seen in stably folded regions (11). In comparison, apo R_D showed bimodal distributions at shorter labeling times and binomial distribution after 10-min deuterium labeling times (Fig. S2). Interestingly, the interdomain linker with its characteristic bimodal spectra (residues 171–190) did not show any significant differences upon cAMP binding.

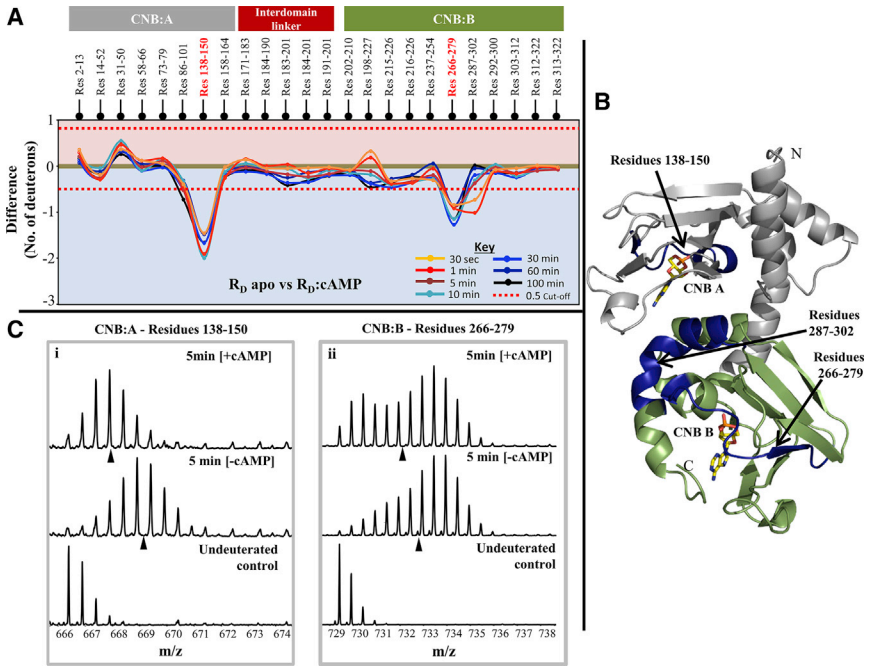

FIGURE 3 Effects of cAMP binding on R_D dynamics. (*A*) Difference plot, plotting absolute difference in deuterons (*y* axis) between apo R_D and R_D:cAMP for each pepsin fragment peptide listed from the N- to C-terminus (*x* axis). Points in the negative scale (shaded *blue*) represent a decrease in deuterium exchange upon cAMP binding, while points in the positive scale (shaded *red*) represent increases in deuterium exchange upon cAMP binding. Peptides spanning the cAMP binding pocket in CNB:A and B are highlighted (in *red*). Each deuterium labeling time for every peptide is depicted and colored according to key. A difference of ± 0.5 Da is considered significant (*red dashed line*). Plots were generated using the software DYNAMX. (*B*) Regions showing significant decreases in deuterium exchange are mapped (*blue*) onto the modeled structure of R_D. cAMP molecules are represented in the structure (*yellow sticks*). (*Gray*) CNB:A (residue 1–180) domain and (*green*) CNB:B domain (residues 181–327); the N- and C-termini of the protein and CNB pockets in A and B domain are labeled. (*C*) Stacked mass spectra of peptides spanning residues (*i*) 138–150 in CNB-A and (*ii*) 266–279 in CNB-B are shown. Mass spectra compares the ligand free state to the ligand bound at 5-min deuterium labeling time. (*Black triangles*) Centroids for the spectra.

R_D and $RegA_C$ form a stable ternary complex with cAMP

In a previous study, we monitored $RegA_C$ mediated cAMP dissociation in mammalian R-subunit prebound to a nonhydrolyzable cAMP analog (Sp-cAMPS) by HDXMS and observed a short-lived ternary complex of R_D:$RegA_C$:Sp-cAMPS (16). The main goal of this study was to characterize the dynamics of the ternary complex in greater detail to gain important insights into how the cAMP signal termination pathway is initiated. R_D was added at a threefold molar excess to $RegA_C$ in the presence of 300 μM cAMP to prime formation of the termination complex. Simultaneous addition of the two proteins with cAMP in the deuterium labeling reaction allowed us to monitor the time-course dependent kinetics/dynamics as the reaction progresses, eventually leading to ternary complex formation. The rationale behind using excess R_D was to channel all of the $RegA_C$ toward complex formation and to obviate any hydrolysis of cAMP by unbound $RegA_C$ in the experiment.

HDXMS results from the R_D:$RegA_C$ complex in the presence of cAMP provide conclusive evidence for a stable ternary complex at the same loci. Importantly, regions in CNB:B of R_D showed decreased exchange for the entire time course of the experiment in the ternary complex. HDXMS results, comparing the ternary complex with R_D:cAMP, are summarized in Fig. 4 *A* in a difference plot. It was also seen that the interdomain linker showed increased exchange. Interestingly, we also observed decreased deuterium exchange at cAMP binding pocket at domain A (residues 138–150) in the ternary complex, at longer labeling times.

The results from the HDXMS experiment were mapped onto the modeled structure of R_D in Fig. 4 *B*. Close examination of the structure showed that the interaction interface can be localized to the cAMP binding pocket of CNB:B. Increased dynamics in the C-helix suggests a mode for allosteric communication between the two cAMP binding pockets. Further confirmation of the stable nature of the ternary complex came from observing the bimodal spectra at residues 266–279. Surprisingly, bimodality was almost negligible, with the entire population shifting to the lower-exchanging, ordered conformation (Figs. 4 *C* and 6 *D*). Deuterium exchange plots also depict the large differences in deuterium exchange between the R_D:cAMP and ternary complex (Fig. 4 *C*).

$RegA_C$ forms a transient complex with R_D in the absence of cAMP

Previously we had shown that the mammalian PKA regulatory subunit (PKAR)-PDE interaction interface between the cAMP binding pocket of mammalian PKAR and the catalytic pocket of PDE is indicative of active site coupling (19,27). While these complexes represent stable endpoint complexes, we set out to monitor the dynamics of the R_D-$RegA_C$ complex by HDXMS experiments with R_D at a threefold molar excess to $RegA_C$ in the absence of excess cAMP. ITC experiments revealed no detectable binding

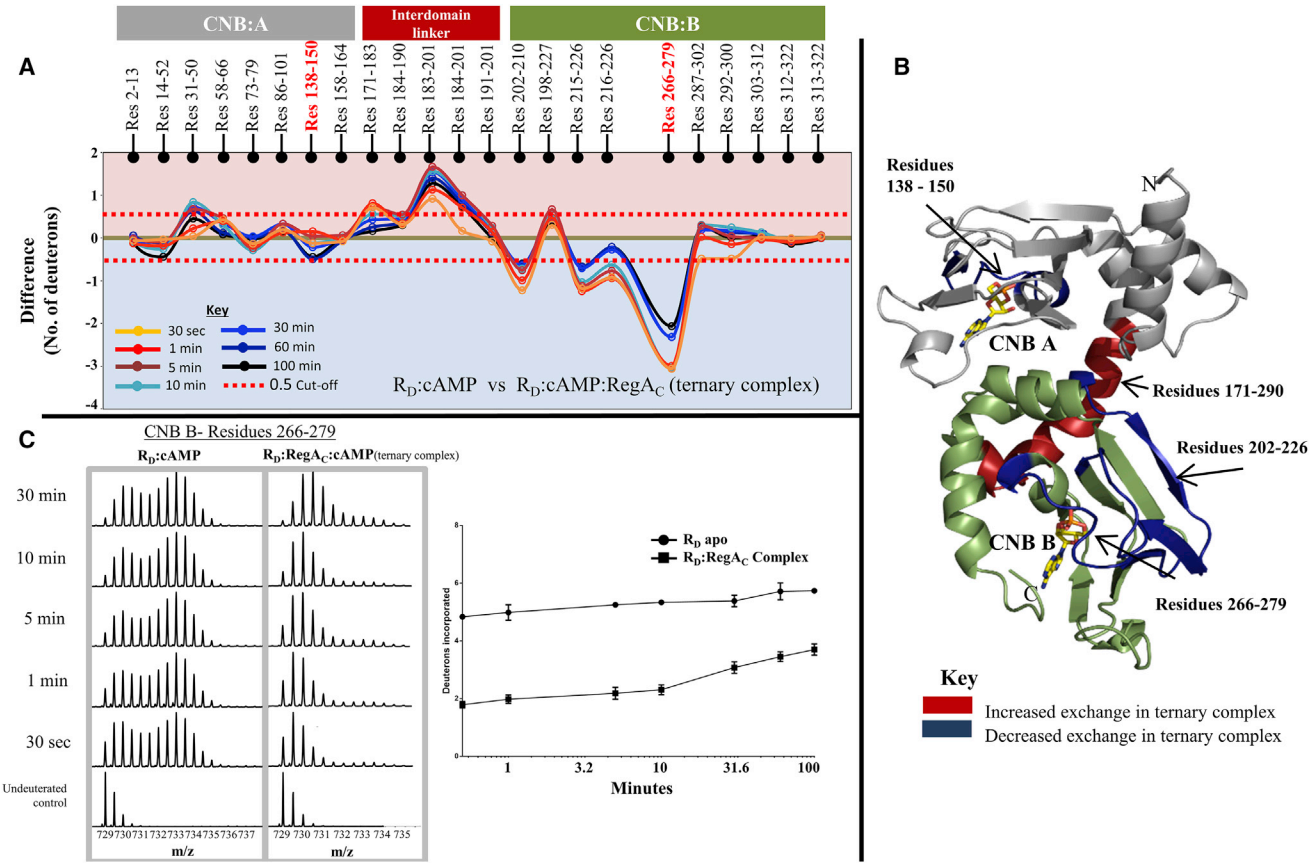

FIGURE 4 Mapping the R_D:$RegA_C$:cAMP ternary complex by HDXMS. (*A*) Difference plot, plotting absolute difference in deuterons (*y* axis) between R_D:cAMP and the R_D:cAMP:$RegA_C$ ternary complex for each pepsin fragment peptide listed from the N- to C-terminus (*x* axis). Points in the negative scale (shaded *blue*) represent a decrease in deuterium exchange in the ternary complex, while points in the positive scale (shaded *red*) represent increases in deuterium exchange. Peptides spanning the cAMP-binding pocket in CNB A and B are highlighted (*red*). Each deuterium labeling time for every peptide is depicted and colored according to key. A difference of ± 0.5 Da is considered significant (*red dashed line*). Plots were generated using the software DYNAMX. (*B*) Regions showing significant differences in deuterium exchange in the ternary complex are mapped onto the modeled structure of R_D according to key. (*Yellow sticks*) cAMP molecules. (*Gray*) The CNB A (residues 1–180) domain and (*green*) CNB B domain (residues 181–327); the N- and C-termini of the protein and CNB pocket in A and B domain are labeled. (*C*) (*Left panel*) Stacked mass spectra of peptides spanning residues 266–279 in CNB-B domain of R_D. Bimodal spectra from R_D:cAMP are compared with spectra from the ternary complex. Mass spectra are stacked in order of increasing deuterium labeling time as shown. (*Right panel*) Deuterium exchange plot comparing R_D:cAMP and R_D:cAMP:$RegA_C$ for the same peptide is depicted. Semilog deuterium exchange plots are generated with *x* axis in the log scale and *y* axis in linear scale; error bars are indicated. Plots are generated in GRAPHPAD PRISM 6 (San Diego, CA).

between $RegA_C$ and apo R_D at the experimental conditions, suggesting that the K_D for the R_D-$RegA_C$ complex to be weaker than 1 μM. Importantly, complex formation was initiated simultaneously with the deuterium exchange reaction to better follow steps in complex formation as well as dissociation. HDXMS results from the binary complex were compared with apo R_D and are presented as a difference plot in Fig. 5 *A*.

Most regions of R_D showed increased deuterium exchange in the presence of $RegA_C$, implying an overall increase in dynamics of R_D in the binary complex. We observed decreased deuterium exchange for many regions in R_D domain B for 30 s and 1-min labeling times, but interestingly, this trend is inversed as labeling time increases, with the same regions showing increased dynamics. These results are consistent with the formation of a R_D-PDE complex with the interaction interface at R_D CNB:B. With increasing labeling time, dissociation of the complex occurs, leading to deuterium exchange even at the interaction interface. While this should eventually result in no differences in deuterium exchange between the apo state and binary complex state, we see increased deuterium exchange at most loci of the CNB-B in the binary complex. Time-dependent differences in deuterium exchange were also observed in contiguous peptides spanning residues 14–52 and 31–50, which showed increased dynamics with increasing reaction time.

We can gain more detailed insights into complex formation and dissociation by using the bimodal spectra as conformational probes, to monitor the degree of disorder in

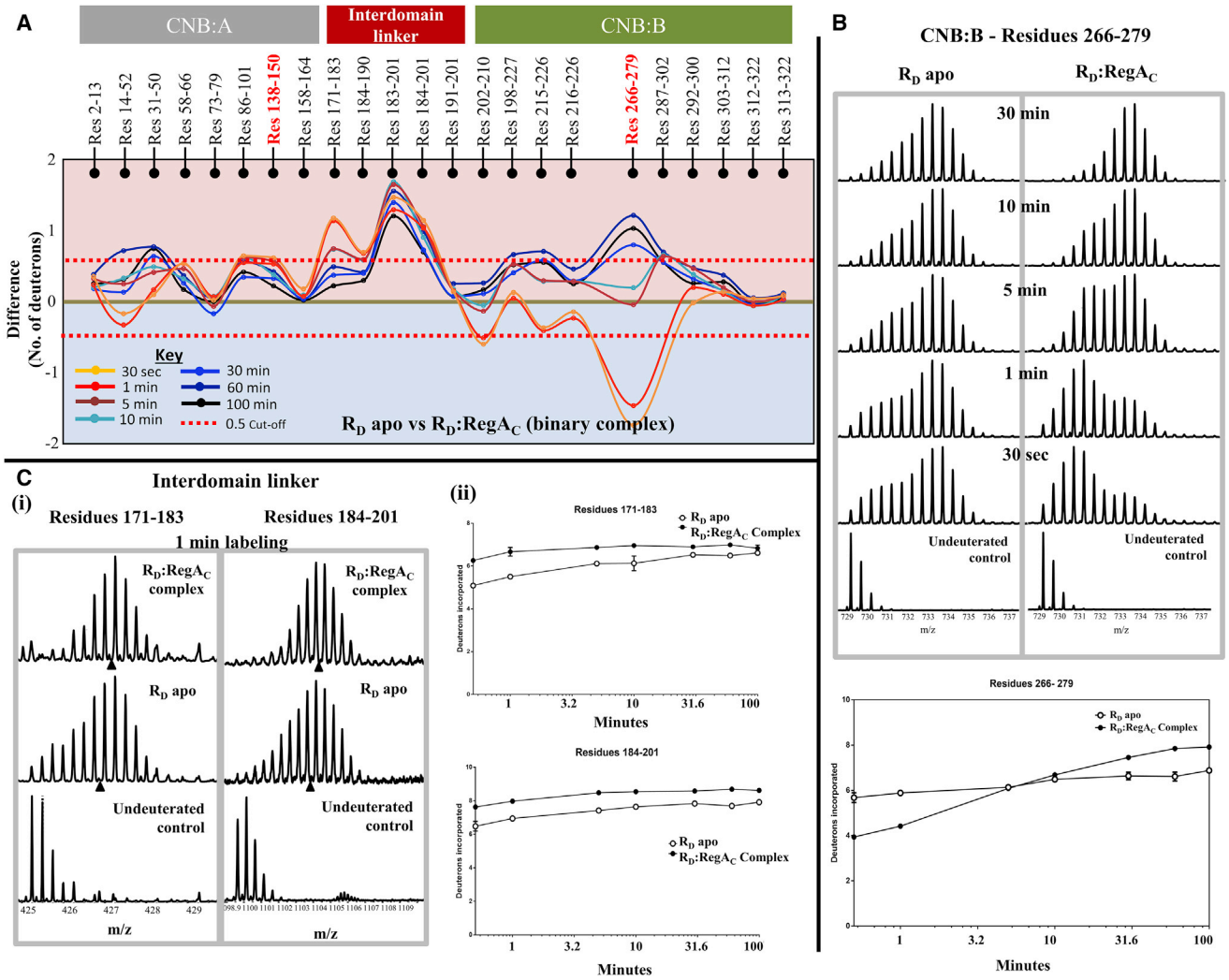

FIGURE 5 Mapping transient R_D:$RegA_C$ interactions by HDXMS. (*A*) Difference plot, plotting absolute difference in deuterons (*y* axis) between apo R_D and R_D:$RegA_C$ binary complex for each pepsin fragment peptide listed from the N- to C-terminus (*x* axis). Points in the negative scale (shaded *blue*) represent a decrease in deuterium exchange upon $RegA_C$ binding, while points in the positive scale (shaded *red*) represent increases in deuterium exchange upon $RegA_C$ binding. Peptides spanning the cAMP binding pocket in CNB:A and B are highlighted (*red*). Each deuterium labeling time for every peptide is depicted and colored according to key. A difference of ± 0.5 Da is considered significant and is shown (*red dashed line*). Plots were generated using the software DYNAMX. (*B*) (*Top panel*) Stacked mass spectra of peptides spanning residues 266–279 in CNB-B domain of R_D. Bimodal spectra from apo R_D are compared with bimodal spectra from the binary complex. Mass spectra are stacked in order of increasing deuterium-labeling time as shown. (*Bottom panel*) Deuterium exchange plot comparing apo R_D and R_D:$RegA_C$ for the same peptide is depicted. (*C*) Representative mass spectra and deuterium exchange plots for two peptides spanning residues 171–183 and 184–201 are shown comparing R_D apo state and R_D:$RegA_C$ state. Semilog deuterium exchange plots are generated with *x* axis in the log scale and *y* axis in linear scale; error bars are indicated. All plots are generated in GRAPHPAD PRISM 6.

residues 266–279. While ligand binding did not result in a significant ordering of structure in this region, $RegA_C$ binding results in significant ordering in early stages of the reaction. As the reaction progressed, the degree of disorder increased and by the end of the reaction (100 min labeling), the peptide is completely deuterated (relative deuterium uptake is ~0.7), suggesting complete disorder in this region (Fig. 5 *B*, *top panel*). This inversion is better visualized in deuterium uptake plots (Figs. 5 *B*, *bottom panel*, and 6 *C*).

We next probed conformational changes associated with complex formation at CNB:A. The bimodal spectra at the interdomain linker (residues 171–190) serve as conformational probes to monitor interconversion of various short-lived conformations of the interdomain linker. As described in the previous section, cAMP binding had no significant effects at the interdomain linker, but $RegA_C$ binding resulted in increased disorder in the linker. We can infer this increased disorder from mass spectral envelopes of peptides from this region (Fig. 5 *C i*). When comparing mass spectra for apo R_D with R_D:$RegA_C$ binary complex, we see the apo spectra showed greater bimodality indicative of residual structure. Upon $RegA_C$ binding, this residual structure is

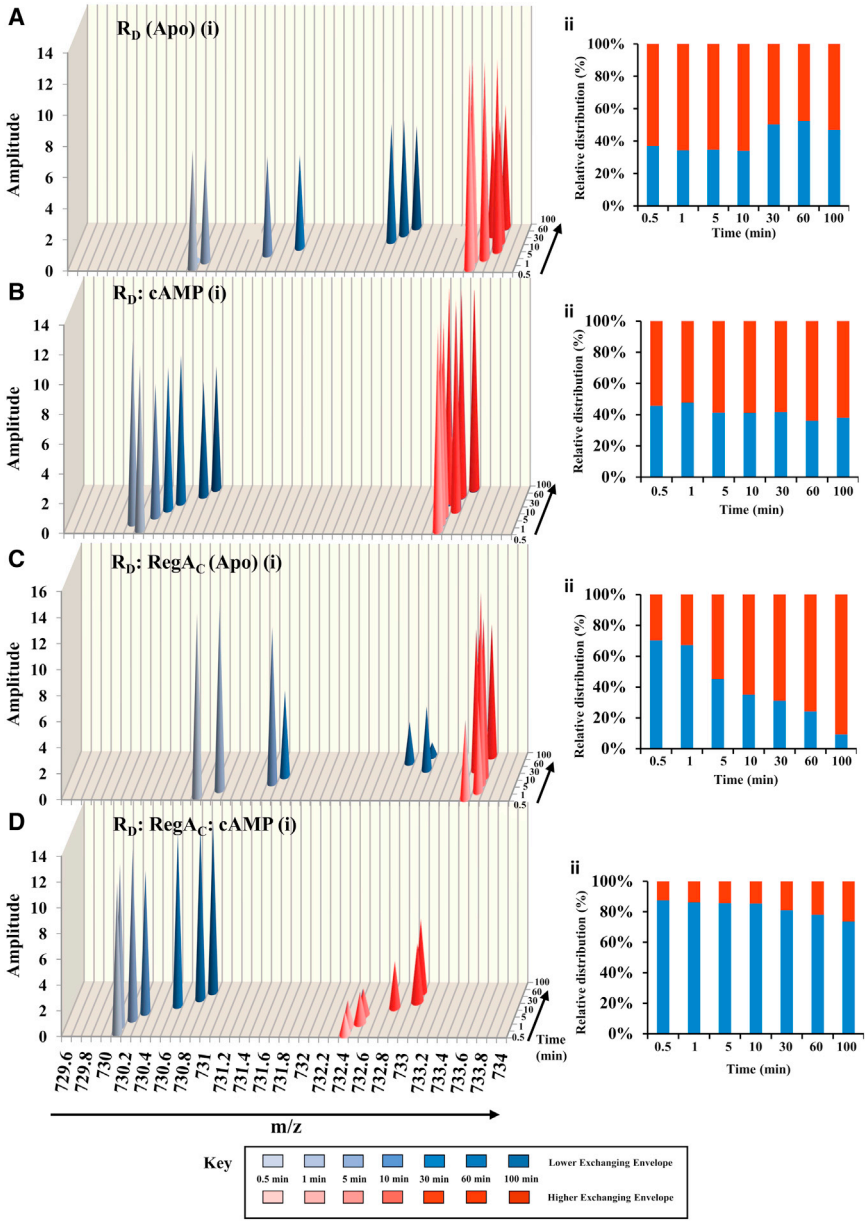

FIGURE 6 Deconvolution of EX1 deuterium exchange kinetics for a CNB:B domain peptide (residues 266–279). Stacked three-dimensional graphs represent the distribution of the bimodal kinetics of the R_D in its different conditions. (*A*) apo R_D; (*B*) R_D with excess of cAMP; (*C*) R_D:$RegA_C$ binary complex in absence of ligand; and (*D*) R_D:$RegA_C$:cAMP ternary complex. Each peak depicts average amplitude value (*y* axis) for the respective centroid values (*x* axis) of the lower-exchanging (shades of *blue*) and higher-exchanging envelopes (shades of *red*) at different time points (*Z* axis). The intensities of the two populations were calculated using an equation for the sum of two Gaussians on GRAPHPAD PRISM 6.0. Relative envelope distributions (percentages) were calculated by normalizing the intensities of peaks from each envelope relative to sum total intensities. *Y* axes represent percentage of the normalized intensities and *x* axes show deuterium exchange (min). (*Blue bars*) Relative intensities of the distribution of lower-exchanging envelopes; (*red bars*) those for the higher-exchanging envelope. The corresponding intensities and deuterium exchange values are listed in Table S2.

eliminated and we observe a binomial distribution corresponding to increased dynamics. Deuterium exchange plots show that this increased dynamics is observed for the entire time course of the experiment (Fig. 5 *C ii*).

These results indicate that $RegA_C$ binds to R_D at CNB:B and causes ordering in R_D domain B while simultaneously inducing long-range conformational changes in domain A as perceived by increased dynamics in domain A. Ordering in CNB:B is transient, and with increases in reaction time, we observed increased overall dynamics across most regions of R_D, providing evidence for the transient nature of the R_D:$RegA_C$ interaction in the absence of cAMP. While cAMP binding showed local effects in deuterium exchange at the cAMP binding pocket, $RegA_C$ binding has a proteinwide effect, providing a case for $RegA_C$-mediated allosteric effects on R_D.

Deconvolution and quantitation of EX1 kinetics at cAMP binding pocket of CNB:B

EX1 kinetics at the cAMP binding pocket of CNB:B were quantitated by deconvolution of the bimodal spectra to obtain centroid and amplitude values for the low-exchanging and high-exchanging envelopes. The key parameters in quantitating EX1 kinetics data are the amplitude ratios between the envelopes, centroids of each envelope, and the changes with respect to time. The quantitated data are summarized in Fig. 6.

In apo R_D, the centroid of the lower-exchanging envelope shifts with time while the higher-exchanging envelope stays constant (Fig. 6 *A*). Upon addition of cAMP, it is seen that the centroids of both the lower- and higher-exchanging populations stay constant with time (Fig. 6 *B*). In the R_D:$RegA_C$ binary complex, it is once again seen that the centroid of the lower-exchanging population shifts with time (Fig. 6 *C*). In the binary complex, the amplitude ratio shows an inversion with time with lower-exchanging population predominating at earlier time points and the higher-exchanging population predominating at higher time points (Fig. 6 *C ii*). R_D:$RegA_C$:cAMP ternary complex data shows that the lower-exchanging population predominates through the entire time course and the centroids stay constant with time (Fig. 6 *D*). These results highlight the role of cAMP in stabilizing conformations and preventing interchange between the different conformations of R_D.

DISCUSSION

In this study we set out to monitor steps in the cAMP signal termination pathway by probing the dynamic interplay between phosphodiesterases and the regulatory subunit of PKA. We have used HDXMS as a tool to study complex formation and dissociation by monitoring protein dynamics as a function of reaction time. These results build on previous work mapping PDE-R-subunit interactions (27) with evidence for substrate channeling in the PKA R-subunit-PDE signaling complex. Importantly, these results also give key insights into PDE-mediated allosteric regulation in cAMP signal termination. While this work was carried out with proteins from a lower eukaryote, *D. discoideum*, the broad conservation of the components in the cAMP signaling pathway suggests that these results provide a universal model for the various steps in cAMP signal termination pathway.

Steps in the PDE-mediated cAMP signal termination pathway

Our previous work has proposed active site coupling and substrate channeling as a mode for signal termination, whereby PDEs interact with the active site of R_D and hydrolyze cAMP bound to the receptor (27). Here we have deciphered how complex formation and dissociation occurs in the various stages of the cAMP signal termination pathway.

After cAMP-mediated activation of the PKA, the high local concentrations of cAMP would prevent reassociation of the PKA holoenzyme. Thus signal termination would occur only when cAMP is depleted by the action of phosphodiesterases. We have shown here that, in the presence of high concentrations of cAMP, R_D and $RegA_C$ form a stable ternary complex at CNB:B of R_D, which also causes increased exchange at important loci in CNB:A. This is further corroborated by deconvolution analysis of EX1 kinetics observed for a peptide spanning residues 266–279 in CNB:B domain (Fig. 6). The envelope distribution in this peptide is distinct for the ternary complex and is not merely a sum of profiles seen for the R_D:$RegA_C$ and R_D:cAMP states. This is inferred from the greatly diminished profile for the higher-exchanging envelope seen in this condition, compared to the R_D:$RegA_C$ and R_D:cAMP states. This provides important evidence for formation of a stable ternary complex in cAMP signal termination and warrants further characterization. Formation of the ternary complex lends itself to the substrate-channeling model for coordinated cAMP hydrolysis proposed earlier (Fig. 7) (27).

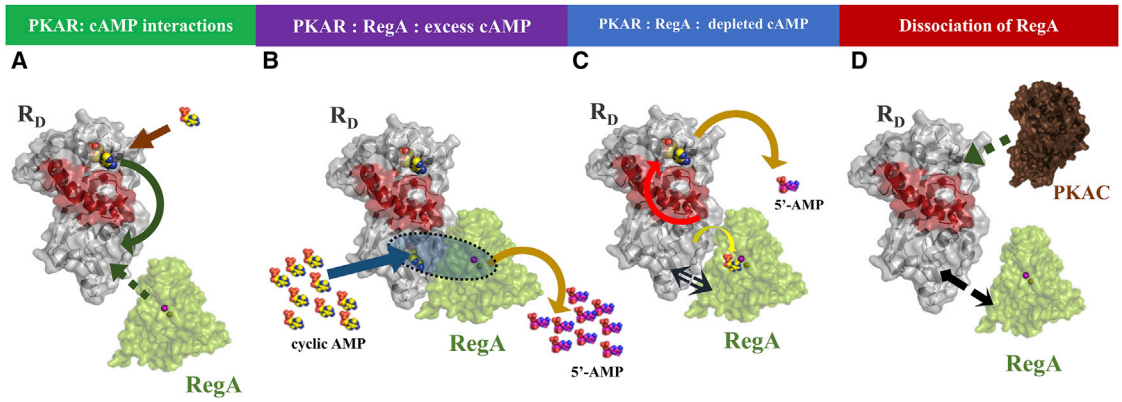

FIGURE 7 Steps in PDE-mediated cAMP signal termination pathway. (*A*) cAMP binding at CNB:A of R_D (in *gray surface representation*) results in an allosteric relay (*green arrow*) that stabilizes structural transitions in CNB:B. This presents an interaction interface for RegA (*green surface representation*) binding. (*B*) In the first step of the cAMP termination pathway, with high local cAMP (in *yellow spheres*) concentrations, R_D and RegA form a stable catalytic complex. cAMP from the local environment binds at the R_D CNB:B cAMP binding pocket and subsequently is channeled into the active site of RegA, as an example for substrate channeling in a signaling complex. (*C*) Once free cAMP is depleted by substrate channeling, RegA and R_D form transient complexes (indicated by the *black arrow*). RegA binding also results in an allosteric relay (*red arrow*) that results in dissociation of cAMP from CNB:A. Thus RegA hydrolyzes all cAMP bound to the receptor and results in apo R_D. (*D*) RegA dissociates from R_D and subsequently primes R_D to reassociate with PKAC resulting in termination of the cAMP signaling pathway. RegA, cAMP, and PKAC serve to regulate R_D through unique allosteric pathways.

The dynamic loci spanning α:C helix and CNBs A and B are involved in allosteric regulation of R_D, and suggest a role for $RegA_C$ in allosterically modulating R_D function. In a cAMP-depleted state, the complex at CNB:B of R_D is transient in nature, but CNB:A exhibits all the allosteric effects observed in the ternary complex. Importantly, increased dynamics is seen at the N-terminal PKAC binding motif of R_D. The dynamics of the PKA binding motif has been shown to play a critical role in tuning PKAC interactions (37). NMR has provided the most detailed insights into the role of the dynamic linkers (51,52) that connect CNB:A and CNB:B domains and have been implicated in both cAMP cooperativity and PKA activation. The α:B-C helical segment serves as more than a passive covalent linker and functions to allosterically respond to cAMP binding to the PBC regions in CNBs A and B (53). Our results indicate that cAMP and $RegA_C$ (PDE) modulate the dynamics of R_D via parallel allosteric pathways.

These results together suggest that in the presence of a large pool of cAMP, the $RegA_C$ and R_D stay associated and function as a stable catalytic multiprotein complex, whereby cAMP that binds to R_D is channeled to the PDE's active site. We predict that this complex would stay stably bound until all cAMP is depleted, suggesting a role for substrate channeling in cAMP signal termination. After depletion of pools of cAMP, the only cAMP molecules left in the system are those associated with R_D receptors. We hypothesize that, without cAMP to stabilize the complex, the PDE forms transient complexes with all R_D molecules in the vicinity. In the process, the PDE dissociates and hydrolyzes all bound cAMP, thereby ensuring signal resetting. Allosteric effects in R_D, particularly at the PKAC binding motif, suggest that the PDE is priming R_D to reassociate with PKAC to terminate the cAMP signaling pathway (Fig. 7). This provides a model for how the cAMP signaling pathway can rapidly reset itself to respond to subsequent stimuli. This also provides a model for how the pathway responds to fluxes of cAMP rather than steady-state levels (54).

Allosteric networks in R_D's role as integrative node in cAMP signaling

HDXMS studies of cAMP-free R_D showed that many regions of the proteins showed a bimodal distribution of mass spectra, specifically the cAMP-binding pocket at CNB:B showed significant bimodal characteristics. Bimodal distributions (EX1 kinetics) are indicative of local unfolding/slow structural transitions, while binomial distributions (EX2 kinetics) are representative of folded states (11). Local unfolding at the cAMP binding pocket provides a structural explanation for the proposed low cAMP affinity at the CNB:B cAMP binding pocket (41,49).

Ligand binding to dynamic proteins is known to shift the equilibrium of a protein from an inactive conformation to an active conformation (2). These effects are more prominent for proteins with disordered regions or in a state of constant structural transitions, with ligand binding causing large-scale ordering in protein structure (7). Thus it was interesting to observe that cAMP did not cause significant ordering at CNB-B, as evidenced from the bimodal nature of the mass spectra. By closely monitoring time-dependent changes in the bimodality of the spectra, it is possible to gain insights into the rate at which structural transitions occur. In apo R_D, the transition from predominantly bimodal to predominantly binomial spectra occurs within 5 min of deuterium exchange reaction. In the cAMP-bound form, although bimodal spectra are observed, the relative ratio of the lower-exchanging and higher-exchanging populations do not change with labeling time (Fig. 6 *B*). This implies that cAMP binding at CNB:A results in a major decrease in the rate of the structural transitions at CNB:B, without causing significant ordering at the binding pocket. The interdomain linker C-helix undergoes drastic conformational changes in mammalian R_D between the cAMP-bound conformation (B-form) and the PKAC-bound conformation (H-form) (32). This helix serves as an important locus for allosteric communication between the two cAMP binding domains (33). In R_D, the interdomain linker region also shows significant local unfolding, but cAMP binding does not have any effect at this loci. These results show cAMP-mediated effects localized mainly to the binding pockets with distinct allosteric communication relays connecting CNB:A to CNB:B.

PDE-mediated effects on R_D are in contrast to cAMP, with $RegA_C$ influencing R_D protein dynamics at many important loci. Importantly, $RegA_C$ causes stabilization of the cAMP binding pocket at CNB:B, as seen from reduced bimodality in spectra in the binary and ternary complex. Furthermore, $RegA_C$ also causes long-range conformational changes that lead to increased dynamics in the interdomain linker of R_D.

Dynamics of R_D play an important in the different stages of the cAMP signaling pathway. The R-subunit has been shown to allosterically respond to both C-subunit binding as well as cAMP (32,33,55–58). These highlight the importance of allostery in the R-subunit for coordinating the activation phase and proceed primarily through CNB:A. Our results reported here indicate the importance of CNB:B in binding PDEs and this interaction is then allosterically coupled to CNB:A through relays that are independent from that mediated by cAMP and the C-subunit. CNB:B domain of R_D from *D. discoideum* is distinct as it has a very low affinity for cAMP compared to the mammalian homologs. Despite this low affinity, our results highlight its importance as a dynamic node for PDE action. This underscores the importance of R-subunits in serving as integrative nodes by coordinating multiple allosteric relays that ultimately govern the output response in both activation and termination phases of the cAMP signalosome (Fig. 7).

SUPPORTING MATERIAL

Four figures and two tables are available at http://www.biophysj.org/biophysj/supplemental/S0006-3495(15)00711-0.

AUTHOR CONTRIBUTIONS

S.K. and N.K.T. designed and performed the experiments; S.K., N.K.T., A.C., and G.S.A. analyzed and interpreted data; and all four authors wrote the article.

ACKNOWLEDGMENTS

This work was supported by grants from the Singapore Ministry of Education Academic Research Fund Tier 3 (No. MOE2012-T3-1-008) and the National University of Singapore awarded to G.S.A.

REFERENCES

1. Gould, C. M., and A. C. Newton. 2008. The life and death of protein kinase C. *Curr. Drug Targets.* 9:614–625.
2. Boehr, D. D., R. Nussinov, and P. E. Wright. 2009. The role of dynamic conformational ensembles in biomolecular recognition. *Nat. Chem. Biol.* 5:789–796.
3. Nussinov, R., and C. J. Tsai. 2014. Unraveling structural mechanisms of allosteric drug action. *Trends Pharmacol. Sci.* 35:256–264.
4. Nussinov, R., C. J. Tsai, and J. Liu. 2014. Principles of allosteric interactions in cell signaling. *J. Am. Chem. Soc.* 136:17692–17701.
5. Gardino, A. K., J. Villali, …, D. Kern. 2009. Transient non-native hydrogen bonds promote activation of a signaling protein. *Cell.* 139:1109–1118.
6. Henzler-Wildman, K., and D. Kern. 2007. Dynamic personalities of proteins. *Nature.* 450:964–972.
7. Smock, R. G., and L. M. Gierasch. 2009. Sending signals dynamically. *Science.* 324:198–203.
8. Moorthy, B. S., and G. S. Anand. 2012. Multistate allostery in response regulators: phosphorylation and mutagenesis activate RegA via alternate modes. *J. Mol. Biol.* 417:468–487.
9. Nussinov, R., B. Ma, and C. J. Tsai. 2014. Multiple conformational selection and induced fit events take place in allosteric propagation. *Biophys. Chem.* 186:22–30.
10. Reynolds, K. A., R. N. McLaughlin, and R. Ranganathan. 2011. Hot spots for allosteric regulation on protein surfaces. *Cell.* 147:1564–1575.
11. Hoofnagle, A. N., K. A. Resing, and N. G. Ahn. 2003. Protein analysis by hydrogen exchange mass spectrometry. *Annu. Rev. Biophys. Biomol. Struct.* 32:1–25.
12. Kaveti, S., and J. R. Engen. 2006. Protein interactions probed with mass spectrometry. *Methods Mol. Biol.* 316:179–197.
13. Englander, S. W., and N. R. Kallenbach. 1983. Hydrogen exchange and structural dynamics of proteins and nucleic acids. *Q. Rev. Biophys.* 16:521–655.
14. Iacob, R. E., J. Zhang, …, J. R. Engen. 2011. Allosteric interactions between the myristate- and ATP-site of the Abl kinase. *PLoS One.* 6:e15929.
15. Sours, K. M., Y. Xiao, and N. G. Ahn. 2014. Extracellular-regulated kinase 2 is activated by the enhancement of hinge flexibility. *J. Mol. Biol.* 426:1925–1935.
16. Krishnamurthy, S., B. S. Moorthy, …, G. S. Anand. 2013. Dynamics of phosphodiesterase-induced cAMP dissociation from protein kinase A: capturing transient ternary complexes by HDXMS. *Biochim. Biophys. Acta.* 1834:1215–1221.
17. Anand, G. S., S. Krishnamurthy, …, D. A. Johnson. 2010. Cyclic AMP- and (Rp)-cAMPS-induced conformational changes in a complex of the catalytic and regulatory (RIα) subunits of cyclic AMP-dependent protein kinase. *Mol. Cell. Proteomics.* 9:2225–2237.
18. Moorthy, B. S., S. Badireddy, and G. S. Anand. 2011. Cooperativity and allostery in cAMP-dependent activation of protein kinase A: monitoring conformations of intermediates by amide hydrogen/deuterium exchange. *Int. J. Mass Spectrom.* 302:157–166.
19. Moorthy, B. S., Y. Gao, and G. S. Anand. 2011. Phosphodiesterases catalyze hydrolysis of cAMP-bound to regulatory subunit of protein kinase A and mediate signal termination. *Mol. Cell. Proteomics.* 10: M110.002295.
20. Mann, S. K., J. M. Brown, …, R. A. Firtel. 1997. Role of cAMP-dependent protein kinase in controlling aggregation and postaggregative development in *Dictyostelium*. *Dev. Biol.* 183:208–221.
21. Firtel, R. A., and A. L. Chapman. 1990. A role for cAMP-dependent protein kinase A in early *Dictyostelium* development. *Genes Dev.* 4:18–28.
22. Shaulsky, G., D. Fuller, and W. F. Loomis. 1998. A cAMP-phosphodiesterase controls PKA-dependent differentiation. *Development.* 125:691–699.
23. Thomason, P. A., D. Traynor, …, R. R. Kay. 1998. An intersection of the cAMP/PKA and two-component signal transduction systems in *Dictyostelium*. *EMBO J.* 17:2838–2845.
24. Taylor, S. S., C. Kim, …, G. S. Anand. 2005. Dynamics of signaling by PKA. *Biochim. Biophys. Acta.* 1754:25–37.
25. Anand, G., S. S. Taylor, and D. A. Johnson. 2007. Cyclic-AMP and pseudosubstrate effects on type-I A-kinase regulatory and catalytic subunit binding kinetics. *Biochemistry.* 46:9283–9291.
26. Johnson, D. A., P. Akamine, …, S. S. Taylor. 2001. Dynamics of cAMP-dependent protein kinase. *Chem. Rev.* 101:2243–2270.
27. Krishnamurthy, S., B. S. Moorthy, …, G. S. Anand. 2014. Active site coupling in PDE:PKA complexes promotes resetting of mammalian cAMP signaling. *Biophys. J.* 107:1426–1440.
28. Mutzel, R., M. N. Simon, …, M. Véron. 1988. Expression and properties of the regulatory subunit of *Dictyostelium* cAMP-dependent protein kinase encoded by λgt11 cDNA clones. *Biochemistry.* 27:481–486.
29. Veron, M., R. Mutzel, …, V. Wallet. 1988. cAMP-dependent protein kinase from *Dictyostelium discoideum*. *Dev. Genet.* 9:247–258.
30. Canaves, J. M., and S. S. Taylor. 2002. Classification and phylogenetic analysis of the cAMP-dependent protein kinase regulatory subunit family. *J. Mol. Evol.* 54:17–29.
31. Berman, H. M., L. F. Ten Eyck, …, S. S. Taylor. 2005. The cAMP binding domain: an ancient signaling module. *Proc. Natl. Acad. Sci. USA.* 102:45–50.
32. Kim, C., C. Y. Cheng, …, S. S. Taylor. 2007. PKA-I holoenzyme structure reveals a mechanism for cAMP-dependent activation. *Cell.* 130:1032–1043.
33. Das, R., V. Esposito, …, G. Melacini. 2007. cAMP activation of PKA defines an ancient signaling mechanism. *Proc. Natl. Acad. Sci. USA.* 104:93–98.
34. Das, R., and G. Melacini. 2007. A model for agonism and antagonism in an ancient and ubiquitous cAMP-binding domain. *J. Biol. Chem.* 282:581–593.
35. McNicholl, E. T., R. Das, …, G. Melacini. 2010. Communication between tandem cAMP binding domains in the regulatory subunit of protein kinase A-Iα as revealed by domain-silencing mutations. *J. Biol. Chem.* 285:15523–15537.
36. Badireddy, S., G. Yunfeng, …, G. S. Anand. 2011. Cyclic AMP analog blocks kinase activation by stabilizing inactive conformation: conformational selection highlights a new concept in allosteric inhibitor design. *Mol. Cell. Proteomics.* 10: M110.004390.
37. Akimoto, M., R. Selvaratnam, …, G. Melacini. 2013. Signaling through dynamic linkers as revealed by PKA. *Proc. Natl. Acad. Sci. USA.* 110:14231–14236.

38. Kornev, A. P., S. S. Taylor, and L. F. Ten Eyck. 2008. A generalized allosteric mechanism for *cis*-regulated cyclic nucleotide binding domains. *PLOS Comput. Biol.* 4:e1000056.

39. Wales, T. E., K. E. Fadgen, …, J. R. Engen. 2008. High-speed and high-resolution UPLC separation at zero degrees Celsius. *Anal. Chem.* 80:6815–6820.

40. Taylor, S. S., J. A. Buechler, and W. Yonemoto. 1990. cAMP-dependent protein kinase: framework for a diverse family of regulatory enzymes. *Annu. Rev. Biochem.* 59:971–1005.

41. Mutzel, R., M. L. Lacombe, …, M. Veron. 1987. Cloning and cDNA sequence of the regulatory subunit of cAMP-dependent protein kinase from *Dictyostelium discoideum*. *Proc. Natl. Acad. Sci. USA.* 84:6–10.

42. Weis, D. D., T. E. Wales, …, L. F. Ten Eyck. 2006. Identification and characterization of EX1 kinetics in H/D exchange mass spectrometry by peak width analysis. *J. Am. Soc. Mass Spectrom.* 17:1498–1509.

43. Konermann, L., and D. A. Simmons. 2003. Protein-folding kinetics and mechanisms studied by pulse-labeling and mass spectrometry. *Mass Spectrom. Rev.* 22:1–26.

44. Wang, L. C., L. K. Morgan, …, G. S. Anand. 2012. The inner membrane histidine kinase EnvZ senses osmolality via helix-coil transitions in the cytoplasm. *EMBO J.* 31:2648–2659.

45. Wildes, D., and S. Marqusee. 2004. Hydrogen-exchange strategies applied to energetics of intermediate processes in protein folding. *Methods Enzymol.* 380:328–349.

46. Engen, J. R., T. E. Smithgall, …, D. L. Smith. 1997. Identification and localization of slow, natural, cooperative unfolding in the hematopoietic cell kinase SH3 domain by amide hydrogen exchange and mass spectrometry. *Biochemistry.* 36:14384–14391.

47. Fang, J., K. D. Rand, …, J. R. Engen. 2011. False EX1 signatures caused by sample carryover during HX MS analyses. *Int. J. Mass Spectrom.* 302:19–25.

48. Su, Y., W. R. Dostmann, …, K. I. Varughese. 1995. Regulatory subunit of protein kinase A: structure of deletion mutant with cAMP binding domains. *Science.* 269:807–813.

49. Degunzburg, J., D. Part, …, M. Veron. 1984. An unusual adenosine 3′,5′-phosphate dependent protein-kinase from *Dictyostelium discoideum*. *Biochemistry.* 23:3805–3812.

50. Houde, D., S. A. Berkowitz, and J. R. Engen. 2011. The utility of hydrogen/deuterium exchange mass spectrometry in biopharmaceutical comparability studies. *J. Pharm. Sci.* 100:2071–2086.

51. Akimoto, M., K. Moleschi, …, G. Melacini. 2014. Allosteric linkers in cAMP signalling. *Biochem. Soc. Trans.* 42:139–144.

52. Popovych, N., S. Sun, …, C. G. Kalodimos. 2006. Dynamically driven protein allostery. *Nat. Struct. Mol. Biol.* 13:831–838.

53. Boulton, S., M. Akimoto, …, G. Melacini. 2014. A tool set to map allosteric networks through the NMR chemical shift covariance analysis. *Sci. Rep.* 4:7306.

54. Leiser, M., N. Fleischer, and J. Erlichman. 1986. Enhanced activation of cAMP-dependent protein kinase by rapid synthesis and degradation of cAMP. *J. Biol. Chem.* 261:15486–15490.

55. Abu-Abed, M., R. Das, …, G. Melacini. 2007. Definition of an electrostatic relay switch critical for the cAMP-dependent activation of protein kinase A as revealed by the D170A mutant of RIα. *Proteins.* 69:112–124.

56. Anand, G. S., C. A. Hughes, …, E. A. Komives. 2002. Amide H/2H exchange reveals communication between the cAMP and catalytic subunit-binding sites in the R(I)α subunit of protein kinase A. *J. Mol. Biol.* 323:377–386.

57. Das, R., M. Abu-Abed, and G. Melacini. 2006. Mapping allostery through equilibrium perturbation NMR spectroscopy. *J. Am. Chem. Soc.* 128:8406–8407.

58. Kim, C., N. H. Xuong, and S. S. Taylor. 2005. Crystal structure of a complex between the catalytic and regulatory (RIα) subunits of PKA. *Science.* 307:690–696.

Parallel Allostery by cAMP and PDE Coordinates Activation and Termination Phases in cAMP Signaling

Srinath Krishnamurthy,[1] Nikhil Kumar Tulsian,[1] Arun Chandramohan,[1] and Ganesh S. Anand[1,*]

[1]Department of Biological Sciences, National University of Singapore, Singapore

SUPPLEMENTARY INFORMATION

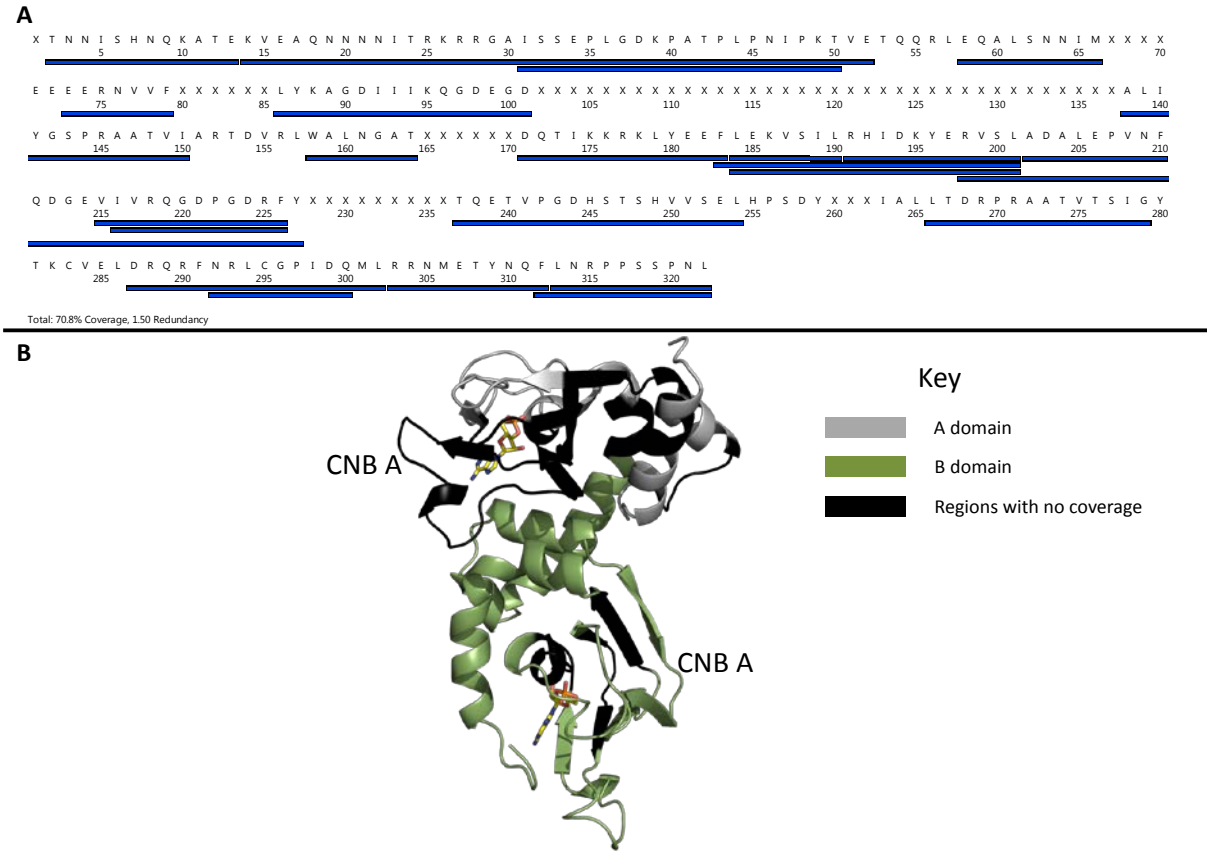

Supplementary Figure 1: ***Sequence coverage of*** R_D**.** A) The primary sequence of full length R_D is depicted. The blue boxes indicate all peptide fragments spanning regions of primary sequence obtained from our data set analysis. Approximately 71% sequence coverage was observed. Amino acids labeled as 'X' are residues which were not identified in the initial protein database search engine. B) Regions with sequence coverage was mapped onto the tertiary structure modelled structure of R_D. CNB-A domain is represented in grey, CNB-B domain is in green and the regions with no coverage in black. Cyclic AMP molecules are shown in yellow sticks.

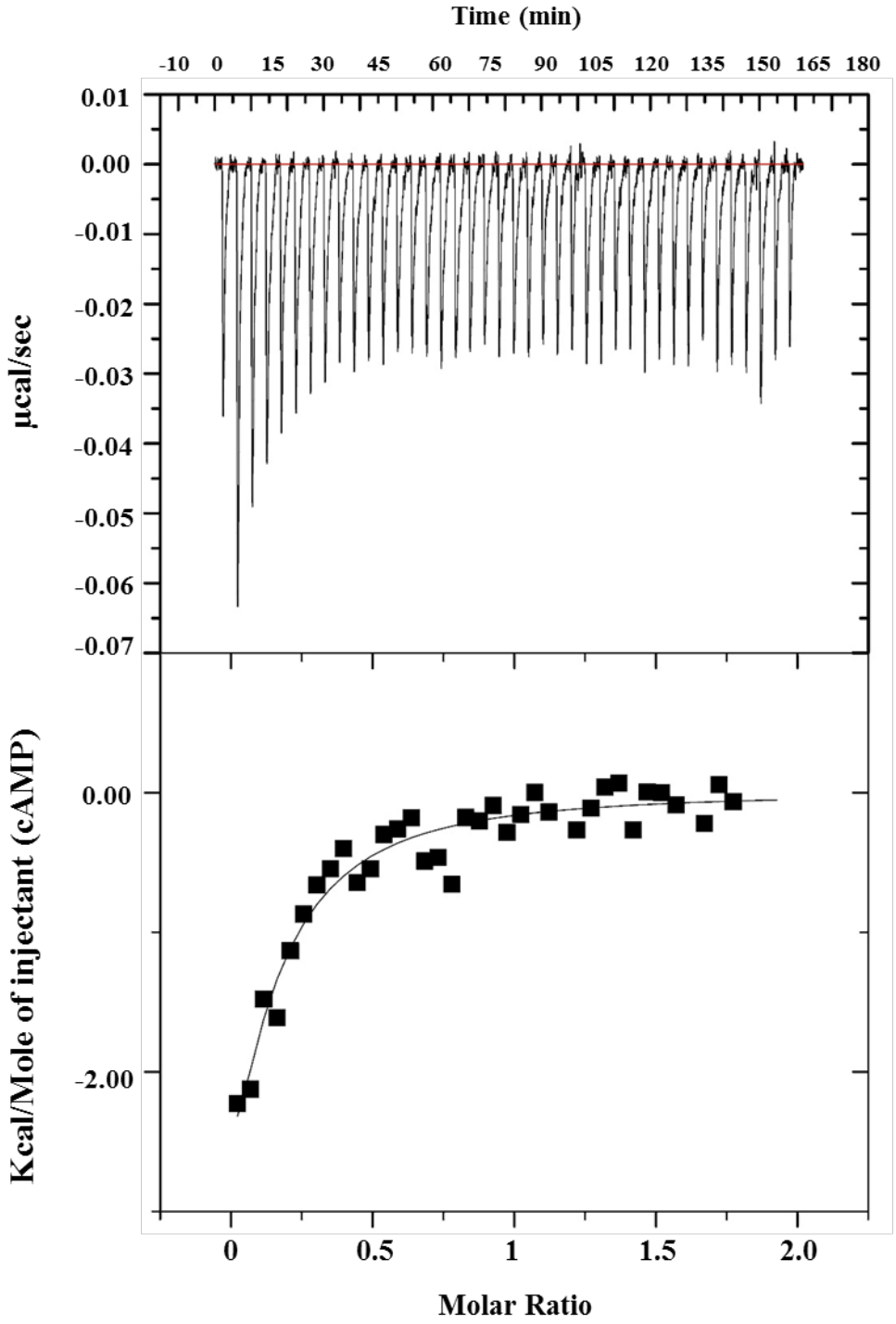

Supplementary Figure 2. cAMP binding to R_D as determined by ITC. Top panel depicts the heat released (and subsequent recovery) upon injection of cAMP from syringe to the experimental cell chamber containing apo R_D protein. For top panel, the observed heat change is plotted on Y-axis (µcal/sec) and X-axis denotes progression of the ITC experiment with time (min). Bottom panel shows the fit of the integrated and corrected heat to a binding isotherm (black line). The release of heat with every injection is plotted on Y-axis (kcal/mole of cAMP) with increase in cAMP/R_D protein molar ratio at X-axis. The fitted values were estimated as ΔH = -53.7 kcal/mol, $K_A = 9.92 \times 10^5\ M^{-1}$.

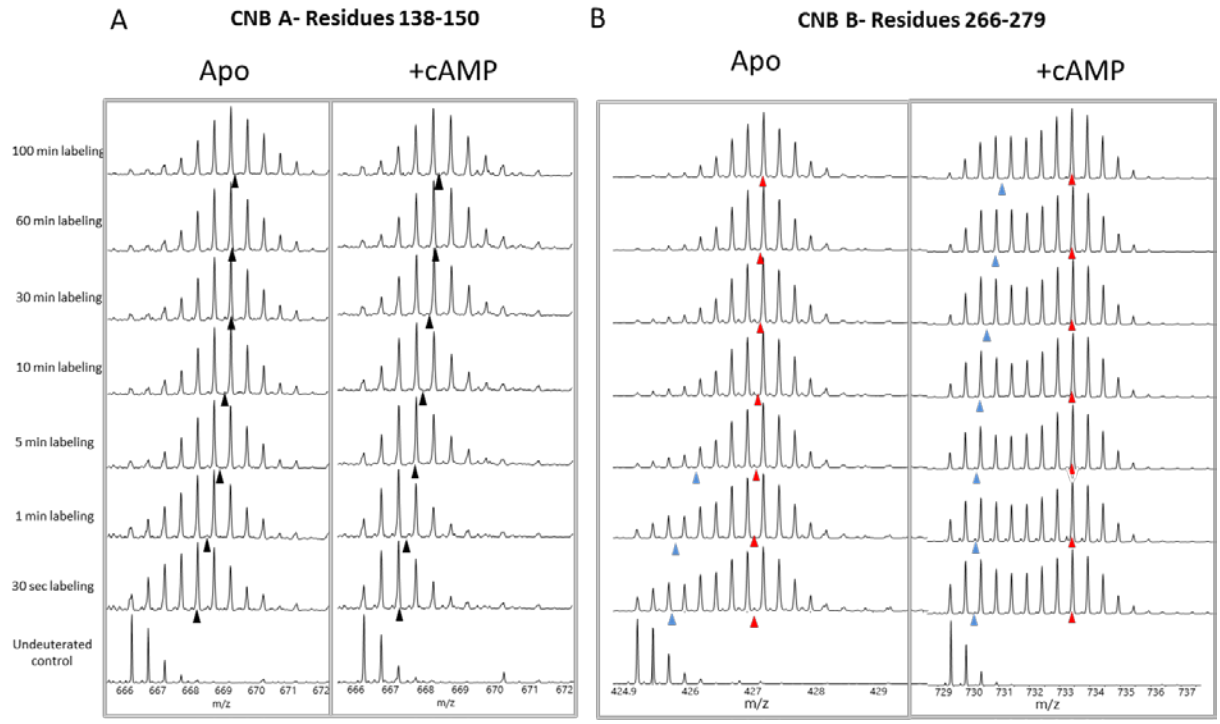

Supplementary Figure 3: ***Comparing dynamics by HDXMS of CNB pockets in cAMP-free (apo) and cAMP bound states:*** A) Stacked mass spectra of a peptide spanning residues 138-150 in CNB-A domain, comparing cAMP-free and cAMP bound state, is depicted with increasing deuterium exchange labeling time. Centroids of the spectrum are labeled in black triangles. B) Stacked mass spectra of peptide fragment spanning residues 266-279 in CNB-B domain, comparing cAMP-free and cAMP bound state, is depicted with increasing deuterium exchange labeling time. Bimodal distributions are seen for shorter labeling times (30 s and 1 min) in apo R_D. In the cAMP bound state, bimodal distribution in mass spectra are seen for all deuterium labeling times. Blue triangles indicate centroid for the lower exchanging envelope and red triangles indicate centroid for the higher exchanging envelope.

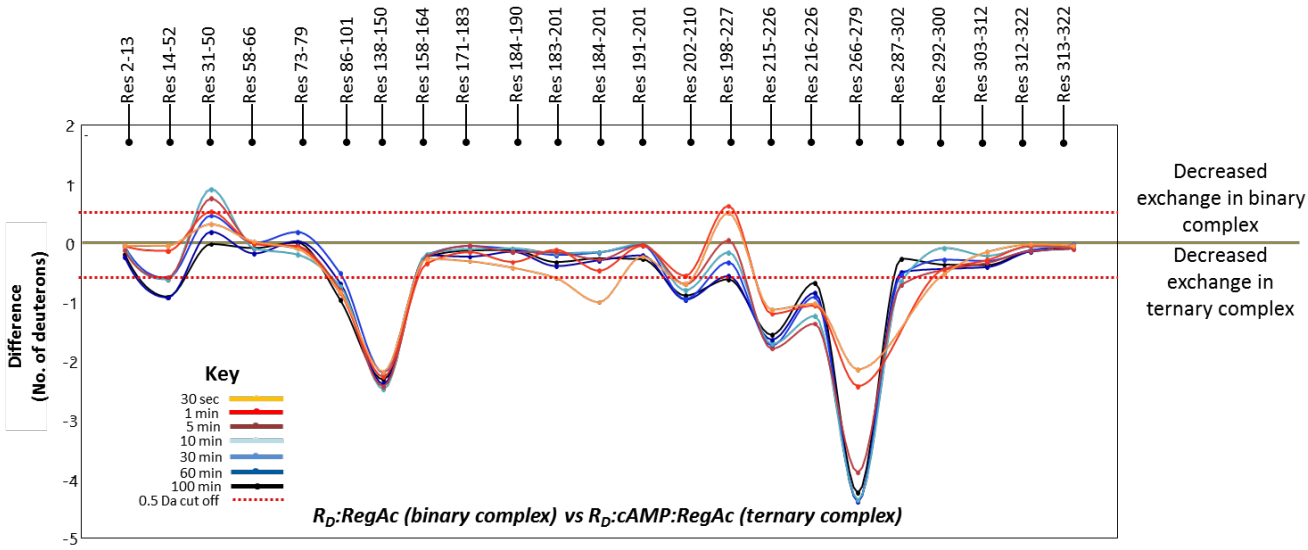

Supplementary Figure 4: A) Difference plot, plotting absolute difference in deuterons (y-axis) between R_D:$RegA_C$ binary state and R_D:cAMP:$RegA_C$ ternary state for each pepsin fragment peptide listed from the N to C-terminus (x-axis). The binary complex and ternary complex are directly compared and points in the negative scale represent a decrease in deuterium exchange in binary complex, while points in the positive scale represent decreases in deuterium exchange of the ternary complex. Each deuterium labeling time for every peptide is depicted and colored according to key. A difference of ±0.5 Da is considered significant and is represented by a red dashed line. Plots were generated using DynamX software (Version 2.0, Waters, Milford).

Supplementary Table 1: Summary of peptide fragments from HDXMS data for apo R_D, R_D:cAMP, R_D:$RegA_C$ and R_D:$RegA_C$:cAMP. The table summarizes the relative deuterium exchange values reported for the 24 peptides obtained in our analysis. A comparison of absolute deuterium exchange of the peptides for two different labelling times 1 min and 30 min is tabulated.

S.No	Peptide sequence (MH^+)	Charge (z)	Residue No.s	MEA[a]	No. of deuterons exchanged after 1min (Mean± SD)[b]				No. of deuterons exchanged after 30min (Mean± SD)[b]			
					R_D Apo	R_D: cAMP	R_D: $RegA_C$	R_D:$RegA_C$: cAMP	R_D Apo	R_D: cAMP	R_D: $RegA_C$	R_D:$RegA_C$: cAMP
1	TNNISHNQKATE (1356.65)	2	2-13	11	5.06 ± 0.04	5.36± 0.05	5.29±0.04	5.23±0.05	5.15± 0.06	5.28± 0.08	5.34±0.02	5.27±0.02
2	KVEAQNNNNITRKRRGAISSEP LGDKPATPLPNIPKTVE (4253.311)	5	14-52	33	17.51±0.10	17.22±0.15	17.19±0.06	17.04±0.08	17.51±0.15	17.2± 0.10	17.62±0.12	17.02±0.05
3	ISSEPLGDKPATPLPNIPKT (2075.138)	2	31-50	14	2.01±0.09	2.47±0.22	2.18± 0.02	2.70±0.06	4.79±0.24	5.15±0.18	5.43±0.12	5.88±0.09
4	EQALSNNIM (1019.483)	3	58-66	8	3.36±0.15	3.48±0.08	3.90±0.06	3.87±0.05	4.42±0.15	4.31±0.12	4.67±0.02	4.66±0.01
5	EERNVVF (892.452)	2	73-79	6	1.04±0.05	1.22±0.13	1.11±0.06	1.34±0.09	2.75±0.05	2.72±0.11	2.58±0.03	2.75±0.13
6	LYKAGDIIIKQGDEGD (1734.891)	2	86-101	15	3.18±0.15	2.75±0.06	3.73±0.06	2.87±0.04	4.45±0.19	3.94±0.12	4.79±0.04	4.26±0.06
7	ALIYGSPRAATVI (1331.768)	2	138-150	11	3.67±0.08	1.76±0.05	4.19±0.12	1.91±0.08	4.88±0.07	3.22±0.13	5.21±0.01	2.99±0.17
8	WALNGAT (732.367)	2	158-164	6	2.38±0.04	2.12±0.05	2.45±0.02	2.09±0.03	2.65±0.03	2.48±0.03	2.70±0.02	2.49±0.04
9	DQTIKKRKLYEEF (1697.922)	4	171-183	12	5.51±0.02	5.67±0.07	6.65±0.15	6.48±0.07	6.53±0.09	6.41±0.02	6.90±0.05	6.84±0.04
10	FLEKVSILRHIDKYERVSL (2345.334)	4	183-201	17	6.92±0.23	6.97±0.12	8.22±0.05	8.09±0.10	7.80±0.25	7.44±0.09	9.19±0.05	8.98±0.01
11	LEKVSIL (801.508)	2	184-190	6	2.60±0.03	2.61±0.06	3.28±0.02	2.95±0.02	3.22±0.06	3.05±0.04	3.62±0.03	3.50±0.01
12	LEKVSILRHIDKYERVSL (2198.266)	2	184-201	17	6.93±0.11	6.79±0.11	7.97±0.02	7.49±0.08	7.85±0.09	7.51±0.09	8.58±0.03	8.41±0.06

13	RHIDKYERVSL (1415.775)	3	191-201	10	4.47±0.02	4.42±0.02	4.62±0.04	4.56±0.07	4.73±0.06	4.52±0.02	4.80±0.02	4.75±0.02
14	RVSLADALEPVNFQDGEVIVRQG DPGDRFY (3362.676)	3	198-227	27	6.60±0.08	6.79±0.10	6.65±0.02	7.27±0.05	9.43±0.11	9.05±0.05	9.84±0.05	9.51±0.05
15	ADALEPVNF (975.478)	4	202-210	7	3.53±0.04	3.45±0.05	3.02±0.05	2.45±0.01	3.76±0.05	3.57±0.03	3.87±0.01	2.92±0.02
16	VIVRQGDPGDRF(1358.717)	2	215-226	10	4.39±0.06	4.01±0.09	3.97±0.09	2.76±0.07	4.97±0.09	4.51±0.06	5.55±0.07	3.80±0.04
17	IVRQGDPGDRF (1259.649)	2	216-226	9	3.92±0.06	3.56±0.07	3.69±0.01	2.62±0.06	4.38±0.06	4.03±0.05	4.68±0.01	3.75±0.03
18	TQETVPGDHSTSHVVSEL (1922.909)	3	237-254	16	6.37±0.23	7.35±0.15	n/a	n/a	7.16±0.02	7.95±0.06	n/a	n/a
19	LTDRPRAATVTSIG (1457.807)	2	266-279	12	5.89±0.05	4.97±0.19	4.42±0.09	1.98±0.12	6.66±0.15	5.39±0.16	7.46±0.03	3.07±0.16
20	DRQRFNRLCGPIDQML (1961.98)	3	287-302	15	6.62±0.17	5.62±0.14	n/a	8.25±0.04	7.69±0.18	7.50±0.08	5.64±0.09	7.69±0.15
21	NRLCGPIDQ (1015.499)	2	292-300	7	3.08±0.06	2.97±0.08	3.28±0.04	2.83±0.06	3.61±0.09	3.47±0.25	3.94±0.05	3.64±0.09
22	RRNMETYNQF (1358.627)	2	303-312	9	5.13±0.05	4.98±0.06	5.23±0.04	4.93±0.08	5.37±0.09	5.13±0.05	5.53±0.06	5.22±0.07
23	FLNRPPSSPNL (1241.664)	2	312-322	7	4.06±0.03	4.04±0.03	4.01±0.04	3.95±0.05	4.10±0.04	4.02±0.03	4.06±0.01	3.93±0.06
24	LNRPPSSPNL (1094.595)	2	313-322	6	3.62±0.05	3.58±0.09	3.65±0.03	3.58±0.03	3.63±0.06	3.56±0.06	3.65±0.05	3.61±0.03

[a] Number of maximum available exchangeable amides for each peptide. [b] Average and standard deviation values calculated from three independent deuterium exchange experiments. n/a Deuteron exchange values not available.

Supplementary Table 2. The tables list the calculated values for the amplitude intensities and respective exchange of deuterons as compared with the undeuterated control, for the two types of exchanging envelopes.

(i) Apo R_D

Time	Amp_1	Centroid_1	DEx ± SD	Amp_2	Centroid_2	DEx ± SD
0.5	7.59	730.8	2.12 ± 0.07	12.99	733.6	7.72 ± 0.07
1	6.67	730.9	2.45 ± 0.08	12.83	733.6	7.72 ± 0.08
5	6.30	731.5	3.52 ± 0.09	11.88	733.7	7.92 ± 0.09
10	5.95	731.8	4.12 ± 0.07	11.53	733.8	8.12 ± 0.07
30	7.52	732.7	5.92 ± 0.06	7.44	733.8	8.12 ± 0.06
60	7.34	732.7	6.05 ± 0.07	6.69	733.7	7.92 ± 0.07
100	6.52	732.8	6.25 ± 0.07	7.37	733.7	8.05 ± 0.07

(ii) R_D: cAMP

Time	Amp_1	Centroid_1	DEx ± SD	Amp_2	Centroid_2	DEx ± SD
0.5	11.10	730.3	1.19 ± 0.05	13.22	733.3	7.12 ± 0.05
1	12.25	730.2	0.92 ± 0.06	13.44	733.3	7.12 ± 0.06
5	8.94	730.4	1.32 ± 0.05	12.72	733.3	7.25 ± 0.05
10	9.59	730.5	1.52 ± 0.05	13.80	733.4	7.32 ± 0.05
30	9.93	730.6	1.79 ± 0.05	13.89	733.3	7.25 ± 0.05
60	7.67	730.8	2.19 ± 0.08	13.65	733.4	7.39 ± 0.08
100	8.25	730.9	2.32 ± 0.06	13.41	733.5	7.52 ± 0.06

(iii) R_D:$RegA_C$ (Apo)

Time	Amp_1	Centroid_1	DEx ± SD	Amp_2	Centroid_2	DEx ± SD
0.5	14.11	730.9	2.32 ± 0.14	5.97	733.6	7.82 ± 0.14
1	14.26	731.1	2.72 ± 0.10	6.98	733.7	7.92 ± 0.10
5	12.05	731.6	3.65 ± 0.07	14.70	733.7	7.99 ± 0.07
10	6.59	731.7	3.99 ± 0.12	12.25	733.7	8.05 ± 0.12
30	4.89	733.1	6.79 ± 0.14	10.84	733.6	7.85 ± 0.14
60	3.16	732.9	6.39 ± 0.14	9.93	733.6	7.79 ± 0.14
100	1.03	733.1	6.72 ± 0.16	10.11	733.7	7.99 ± 0.16

(iv) RD:RegAC:cAMP

Time	Amp_1	Centroid_1	DEx ± SD	Amp_2	Centroid_2	DEx ± SD
0.5	11.70	730.1	0.65 ± 0.24	1.67	732.4	5.32 ± 0.24
1	12.64	730.1	0.79 ± 0.23	2.03	732.4	5.32 ± 0.23
5	13.24	730.2	1.05 ± 0.17	2.22	732.5	5.52 ± 0.17
10	11.09	730.3	1.19 ± 0.19	1.90	732.5	5.59 ± 0.19
30	13.45	730.6	1.85 ± 0.16	3.15	732.8	6.12 ± 0.16
60	13.44	730.8	2.12 ± 0.14	3.80	733	6.52 ± 0.14
100	13.27	730.9	2.32 ± 0.14	4.76	733	6.59 ± 0.14

All calculations were done using the sum of two Gaussians equation in GraphPad Prism 6.0.

*__Amp_1__: Amplitude, __Centroid_1__: centroid in m/z for +2 charge state mass spectral envelope, __DEx_1± SD__: number of deuterons exchanged and the standard deviations for the lower exchanging envelope; **__Amp_2__: Amplitude, __Centroid_2__: representative m/z value of centroid peak for +2 charge state, __DEx_2± SD__: number of deuterons exchanged and their standard deviations for the higher exchanging envelope. Each data point represented is an average of minimum of three independent experimental values.